Fractional derivative-based approximation of acoustic waveform dispersion measured in bubbly water beyond resonance frequency

Yves Le Gonidec

JASA ARTICLE

Fractional derivative-based approximation of acoustic waveform dispersion measured in bubbly water beyond resonance frequency

Yves Le Gonidec[a)]
Université de Rennes, CNRS, Géosciences Rennes, UMR 6118, 35000 Rennes, France

ABSTRACT:
Acoustic pulses transmitted across air bubbles in water are usually analyzed in terms of attenuation coefficient and phase velocity in the frequency domain. The present work expresses an analytical approximation of the acoustic waveform in the time domain. It is introduced by experiments performed with a Gaussian derivative source wavelet, $S_0(t)$, with a derivative order, $\beta_0 = 4$, and a peak frequency, ν_{p_0}, much larger than the bubble resonance frequency. The measurements highlight a significant shape variability of the waveform $B_x(t)$, measured at $x \leq 0.74$ m and characterized by a peak frequency $\nu_{p_x} \simeq \nu_{p_0}$. The results are in good agreement with the approximation $B_x(t) \propto (d^{\gamma_x}/dt^{\gamma_x}) S_0(\delta_x t - T)$, where γ_x is an additional fractional-derivative order determined by an optimization procedure and T is related to the travel time. The time-scale parameter, $\delta_x = \sqrt{\beta_0/(\beta_0 + \gamma_x)}$, becomes a free parameter for more general source signals. The correlation coefficient between $B_x(t)$ and the approximated waveform is used to identify the applicability of the method for a wide range of bubbly waters. The results may be of potential interest in characterizing gas bubbles in the ocean water column and, more generally, in modeling wave propagation in dispersive media with fractional-derivative orders in the time domain. © *2023 Acoustical Society of America*.
https://doi.org/10.1121/10.0022256
(Received 14 July 2023; revised 10 October 2023; accepted 11 October 2023; published online 2 November 2023)
[Editor: Nicholas P. Chotiros] Pages: 2812–2820

I. INTRODUCTION

In underwater acoustics, a wave may be drastically affected by the presence of bubbles, which may act as strong scatterers (Ainslie and Leighton, 2011). A single bubble is characterized by a low-frequency resonance, ν_r, typically 3 kHz for a 1 mm radius air bubble in water as initially quantified in the 1930s by Minnaert and extensively considered since then (Ammari *et al.*, 2018; Devaud *et al.*, 2008). For a bubble cloud, the bubbly water is characterized by an effective complex wavenumber, where real and imaginary parts are related to the phase velocity, $v(\nu)$, and attenuation coefficient, $\alpha(\nu)$, respectively. Many physical phenomena and bubble properties can be considered when modeling v and α, including multiple scattering and bubble-bubble interactions (Ando *et al.*, 2009; Doc *et al.*, 2016; Fuster *et al.*, 2014; Rubinstein, 1985; Valier-Brasier *et al.*, 2015), encapsulating shell and bubble shape (Frinking *et al.*, 1999; Hoff *et al.*, 2000; Liang *et al.*, 2008; Padilla and Weber, 2021), and polydispersity (Fan *et al.*, 2019). Because of this complexity, various experimental works have been performed for many years to measure v and α and compare the results with effective models in the frequency domain (Commander and Prosperetti, 1989; Fox *et al.*, 1955; Goertz *et al.*, 2006; Silberman, 1957; Wilson *et al.*, 2005).

Some publications illustrate the acoustic signals in the time domain (Duraiswami *et al.*, 1998; Duro *et al.*, 2011; Leroy *et al.*, 2008; Suiter, 1992). For instance, Leroy *et al.* (2008) show a 50 kHz acoustic pulse transmitted through a bubbly gel composed of 0.15% volume fraction of 81 μm radius bubbles: the shape of the transmitted signal is more complex than the pulse shape. A quantitative relationship between this complexity and the dispersive character of the bubbly gel is not obvious because the measurement had been performed near resonance, where attenuation and phase velocity change significantly with the frequency (Foldy, 1945). For a weak attenuation that linearly increases with the frequency (Futterman, 1962), waveform changes can be attributed to fractional integration effects (Ker and Le Gonidec, 2018). This may not be the case in the bubbly medium at frequencies far beyond the bubble resonance frequency where the attenuation is weak but follows a decreasing trend with the frequency. In the present work, a 310 kHz acoustic pulse propagates in bubbly water composed of roughly 0.2% volume fraction of 1.6 mm radius air bubbles ($\nu_r \simeq 2$ kHz): the study focuses on analytical descriptions of phenomenological effects that affect the acoustic waveform.

The laboratory acoustic experiments are described in Sec. II to introduce qualitative changes of the acoustic waveforms associated with a propagation distance $x \leq 740$ mm inside the bubbly water. The attenuation coefficient, $\alpha(\nu)$, and phase velocity, $v(\nu)$, are measured in the frequency domain to be compared with effective models. Section III deals with the methodology developed in the framework of Gaussian derivative properties with a source

a)Email: Yves.LeGonidec@univ-rennes.fr

https://doi.org/10.1121/10.0022256

wavelet characterized by a derivative order, β_0, and peak frequency, ν_{p_0}: it introduces a fractional-derivative order and a time-scale factor to approximate the acoustic waveform in the time domain and numerically compares the results with theoretical waveforms. In Sec. IV, the approach is applied to the experimental waveforms measured in the water tank, and discussions concern the applicability range by extending the analyzing to general bubbly waters. Section V deals with the conclusion and potential interests of the method, in particular, for gas bubbles in the ocean water column.

II. EXPERIMENTS IN AN ACOUSTIC WATER TANK

A. Acoustic waveforms

Experiments are performed in an acoustic tank filled with 5 m^3 of water. A piezo-electric transducer with a central frequency of 500 kHz is used to emit acoustic pulses. A similar transducer is placed in front of the emitter to record the transmitted acoustic signal. The waveform, $S_0(t)$, recorded at the distance $x_0 = 365$ mm represents the reference signal in the following [Figs. 1(a1) and 1(b1)],

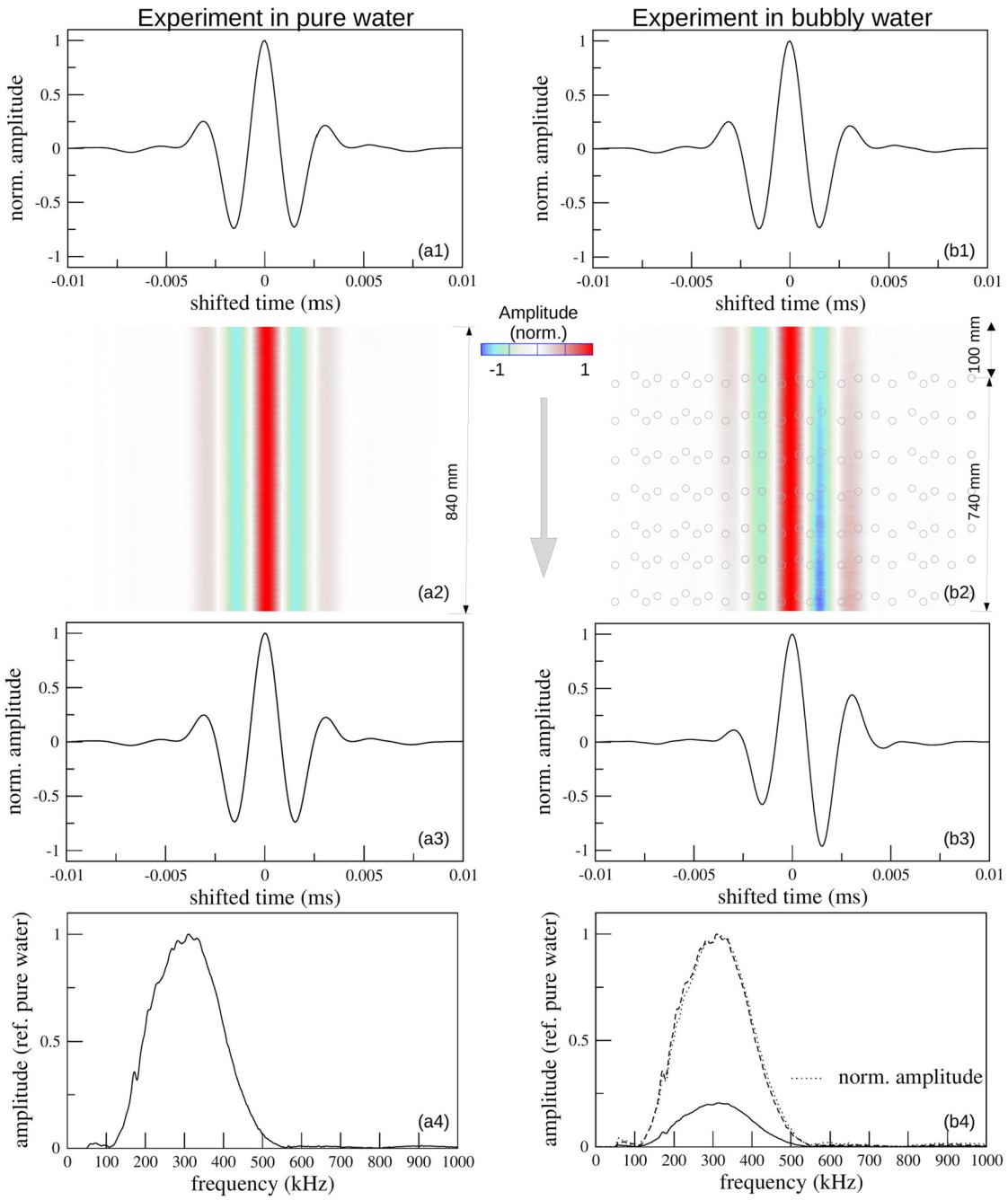

FIG. 1. (Color online) Experimental waveforms measured (left) in pure water and (right) in bubbly water, depicting (a1), (b1) reference source signals and (a2), (b2) transmitted waveforms measured at 211 successive positions x. The waveforms are displayed with a normalized amplitude and arbitrary time reference. (a3), (b3) Last transmitted waveforms and (a4), (b4) associated amplitude spectra normalized to the amplitude in pure water (solid curves). Note that the normalized amplitude spectra measured in pure and bubbly waters are similar [(b4), dashed and dotted curves, respectively].

acquired with a sampling rate of 10 MHz. As a first approximation, this waveform is a Gaussian derivative wavelet [see Eq. (14)] composed of five extrema: it is symmetric relative to the main peak, which defines the center of the waveform and is arbitrarily set to one (normalized amplitude at x_0). The signal is defined by a frequency spectrum, $|\hat{S}_0(\nu)|$, which is maximum at the peak frequency, $\nu_{p_0} \simeq 310$ kHz [Fig. 1(a4)].

The first dataset consists of 221 acoustic waveforms, $W_x(t)$, measured in water between x_0 and $x_0 + 840$ mm [Figs. 1(a2)–1(a4)]. By correcting the waveform amplitude from the spherical divergence of the acoustic beam and time shifting the amplitude peak at $t = 0$, the waveforms, $W_x(t)$, are all similar to $S_0(t)$ [Fig. 1(a2)]: in particular, the symmetry of the waveform and the amplitude spectrum do not depend on the distance, x, as expected for a nondispersive medium [Figs. 1(a3) and 1(a4)].

The second dataset consists of 221 acoustic waveforms, $B_x(t)$, measured in bubbly water [Figs. 1(b2)–1(b4)]. Air bubbles are being released in the water by the use of an artificial generator composed of eight parallel identical pierced tubes, 10 cm apart, filled with air under a pressure of 1.4 bars [Fig. 2(a)]. Each tube is 8 mm in diameter and has been pierced with 26 holes, 2 cm apart, to create a bubble cloud in the water. The distance between the acoustic emitter and the first tube is 10 cm, i.e., the recorded waveform at the initial position, x_0, is $B_0(t) = S_0(t)$ [Fig. 1(b1)]. Bubbles are ellipsoidal [Fig. 2(a)], where half minor axes are between 1 and 3 mm and eccentricity is about 1.5 [Fig. 2(b)]. Measurements are not accurate but not critical for the present study, and a bubble is approximated to a fluid sphere whose radius is half the minor axis. A lognormal distribution highlights a median value of $r_0 = 1.6$ mm and a polydispersity $\epsilon = 20\%$ [Fig. 2(c)]. The gas volume fraction of the biphasic medium is estimated from $\frac{4}{3}\pi r_0^3 N_b N_t / V$, where $N_b \simeq 11$ is the number of bubbles in one picture, $N_t = 8$ is the number of tubes, and $V \simeq 1.5$ l is the volume associated with the picture surface multiplied by the length, 740 mm, of bubbly water. As a rough estimate, the bubbly liquid is characterized by 0.15% volume fraction of 1.6 mm radius air bubbles with a 20% polydispersity in water, where the sound speed is about 1473 m s^{-1}.

The mean acoustic field is measured by averaging 200 signals that propagate through different realizations of the dynamic bubbly water. As a key observation, the waveform, $B_x(t)$, depends on the distance, x: the symmetry is progressively lost when x increases from 0 to 740 mm [Figs. 1(b2) and 1(b3)], but the normalized amplitude spectrum is not modified [Fig. 1(b4)]. This highlights qualitative results on the continuous modification of the average acoustic waveform when the acoustic wave propagates inside the dispersive medium.

B. Attenuation coefficient and phase velocity

Based on the acoustic measurements, the bubble-free water can be approximated to a lossless medium compared to the bubbly water, i.e., an acoustic wave of angular

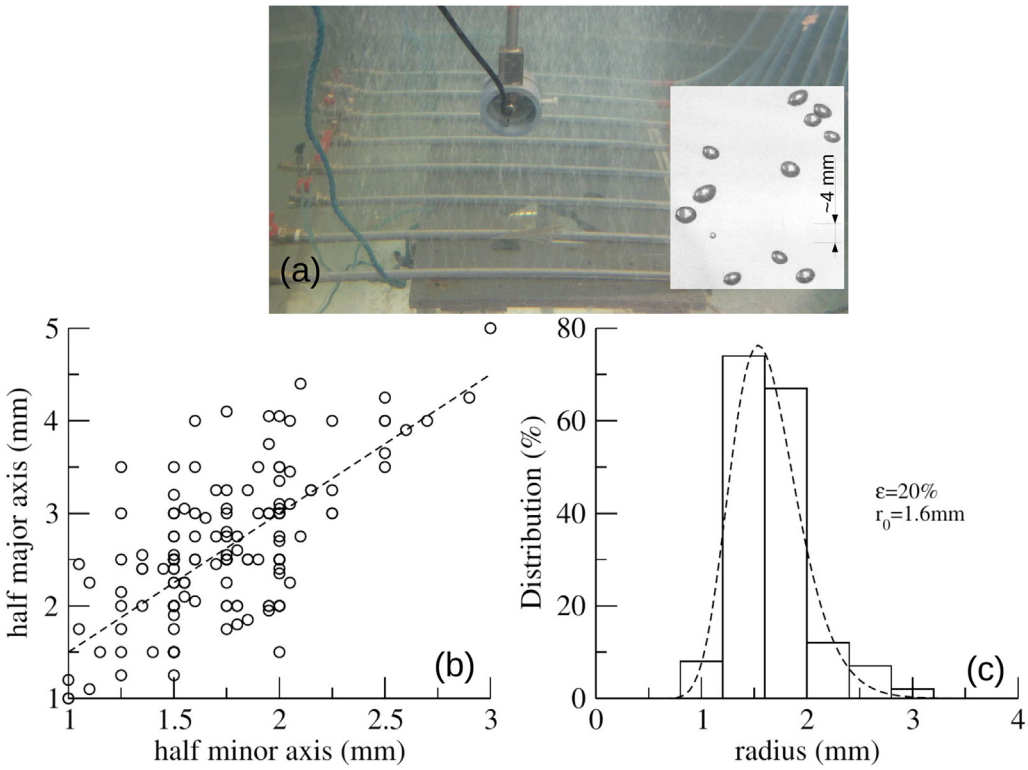

FIG. 2. (Color online) (a) Photographs of the eight bubble clouds and few bubbles (inset picture), (b) major and minor axes of elliptical bubbles (circles), and (c) experimental and lognormal (dashed curve) size distributions are shown.

https://doi.org/10.1121/10.0022256

frequency $\omega = 2\pi\nu$ propagates in water at a constant speed, v_0, with a real wavenumber, $k_0 = \omega/v_0$. In the Fourier domain, the acoustic plane wave measured at x is given by

$$\hat{W}_x(\nu) = \hat{S}_0(\nu)e^{i2\pi\nu(t-x/v_0)}. \tag{1}$$

In the dispersive medium, the acoustic wave propagates with a frequency dependent complex wavenumber, $k(\nu)$, where real and imaginary parts are defined by an attenuation coefficient, $\alpha(\nu)$, and a phase velocity, $v(\nu)$, respectively, according to

$$k(\nu) = \frac{2\pi\nu}{v(\nu)} - i\alpha(\nu), \tag{2}$$

and the acoustic plane wave measured after a propagation distance, x, inside the bubbly water is, thus, given by

$$\hat{B}_x(\nu) = \hat{S}_0(\nu)e^{i(2\pi\nu t - kx)} \tag{3a}$$

$$= \hat{W}_x(\nu)e^{-x\alpha(\nu)}e^{i2\pi\nu(x/v_0 - x/v(\nu))}. \tag{3b}$$

The attenuation coefficient is related to the ratio of the moduli $|\hat{B}_x(\nu)|$ and $|\hat{W}_x(\nu)|$ and the phase velocity to the phase shift, $\Delta\Phi = \arg(\hat{B}_x(\nu)) - \arg(\hat{W}_x(\nu))$, which gives

$$\alpha(\nu) = -\frac{1}{x}\ln\frac{|\hat{B}_x(\nu)|}{|\hat{W}_x(\nu)|}, \tag{4a}$$

$$v(\nu) = \frac{xv_0 2\pi\nu}{x2\pi\nu - v_0\Delta\Phi}. \tag{4b}$$

For frequencies close to $\nu_{p_0} \gg \nu_r$, the experiments highlight very weak dependencies of α and v with ν (Fig. 3, circles).

The complex wavenumber, $k(\nu)$, can be modeled by the use of an effective medium theory. The model developed by Foldy (1945) is widely used in the "independent scattering approximation" for dilute systems and isotropic scatterers with a radius $r < \lambda$: the far-field isotropic scattering amplitude of a single bubble (Ye, 1997) is characterized by the so-called Minnaert frequency, ν_r. For the radius $r_0 = 1.6$ mm, a single bubble resonates at $\nu_r \simeq 2$ kHz, which is much lower than the source peak frequency, $\nu_{p_0} = 310$ kHz. In the model developed by Lax (1951), the isotropic scattering amplitude is replaced by the forward scattering amplitude of a fluid sphere (Anderson, 1950) to take anisotropic scatterers into account when $\lambda < r$.

The complex wavenumbers are computed by considering the physical parameters of the experiment, including the median bubble radius, r_0, and the polydispersity, ϵ: only the volume fraction initially estimated about 0.15% has been increased to $\phi = 0.2\%$ to better fit the model and experimental results. The Foldy model predicts an attenuation that strongly depends on the frequency and underestimates the measurements [Fig. 3(a), dashed curve]: for frequencies as high as $\nu_{p_0} = 310$ kHz, air bubbles with $r_0 = 1.6$ mm cannot be approximated to isotropic scatterers, and this model is not adapted. The theoretical attenuation, $\alpha(\nu)$, and phase velocity, $v(\nu)$, based on the Lax's model are in good agreement with the data [Figs. 3(a) and 3(b), solid curves]: in particular, it correctly predicts the weak decrease in the attenuation coefficient with the frequency. This means that

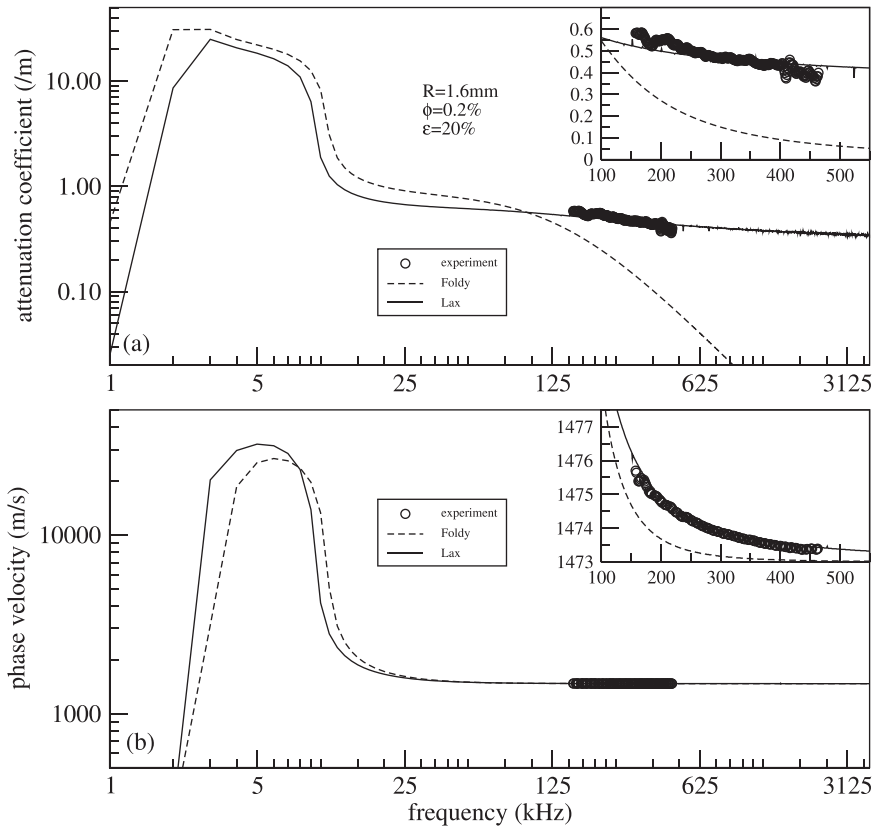

FIG. 3. (a) Experimental attenuation coefficient and (b) phase velocity measured with a source peak frequency $\nu_0 = 310$ kHz across 0.74 cm of bubbly water (circles) and predicted by effective models by Foldy (dashed curve) and Lax (thin curve) are shown.

bubbles act as anisotropic scatterers in the biphasic medium where multiple scattering can be neglected.

III. METHODOLOGY

A. Additional time-derivative order, γ_x, and time-dilation factor, v_x

The reference source signal, $S_0(t)$, is similar to a Gaussian derivative wavelet with a derivative order $\beta_0 = 4$ (Le Gonidec *et al.*, 2002) such that

$$B_0(t) \sim S_0(t) \equiv \frac{d^{\beta_0}}{dt^{\beta_0}} e^{-\pi^2 \nu_0^2 (t-\tau_0)^2}, \tag{5}$$

which is characterized by five extrema and symmetric relative to the maximum peak located at time τ_0, and a natural frequency,

$$\nu_0 = \nu_{p_0} \sqrt{2/\beta_0}, \tag{6}$$

where $\nu_{p_0} = 310$ kHz is the peak frequency. In the frequency domain, the wavelet can be expressed by

$$\hat{S}_0(\nu) = \left(\frac{\nu^2}{\nu_{p_0}^2} e^{1-\nu^2/\nu_{p_0}^2} \right)^{\beta_0/2} e^{i(-2\pi\nu\tau_0 + \pi\beta_0/2)}, \tag{7}$$

and includes the normalization factor of the Gaussian derivative function (Wang, 2015), i.e., $|\hat{S}_0(\nu_{p_0})| = 1$. Inside the bubbly water, the amplitude spectrum of the Fourier transform of the waveform, $B_x(t)$, is

$$|\hat{B}_x(\nu)| = e^{-\alpha(\nu)x} \left(\frac{\nu^2}{\nu_{p_0}^2} e^{1-\nu^2/\nu_{p_0}^2} \right)^{\beta_0/2}. \tag{8}$$

As a main approximation based on the measurements, the attenuation coefficient weakly changes the source peak frequency and

$$|\hat{B}_x(\nu)| \sim |\hat{\tilde{B}}_x(\nu)| = A_x \left(\frac{\nu^2}{\nu_{p_x}^2} e^{1-\nu^2/\nu_{p_x}^2} \right)^{\beta_0/2}, \tag{9}$$

where the factor A_x does not depend on the frequency. In this case, the modified peak frequency, $\nu_{p_x} \simeq \nu_{p_0}$, i.e., the product $\nu_0 \sqrt{\beta_0/2}$ is nearly a constant. Actually, this does not require that the natural frequency and derivative order of the Gaussian derivative wavelet remain constant but may depend on x via $\nu_{p_x} = \nu_{0_x} \sqrt{\beta_x/2}$, associated with the modified derivative order,

$$\beta_x = \frac{\nu_0^2}{\nu_{0_x}^2} \beta_0 = \frac{\beta_0}{\delta_x^2}, \tag{10}$$

where δ_x is equivalent to a time-dilation factor. By introducing the additional derivative order,

$$\gamma_x = \beta_x - \beta_0, \tag{11}$$

this leads to the formulation of the amplitude spectrum,

$$|\hat{\tilde{B}}_x(\nu)| = A_x \left[\left| \hat{S}_0 \left(\frac{\nu}{\delta_x} \right) \right| \left(\frac{\nu}{\nu_{p_0}} \right)^{\gamma_x} \right]^{\delta_x^2}. \tag{12}$$

The relationship between the additional derivative order, γ_x, and the time-scale parameter, δ_x, shows that for $\beta_0 = 4$, δ_x decreases from 1 to 0.98 when γ_x increases from 0 to 0.1. As a first approach, the approximation

$$|\hat{\tilde{B}}_x(\nu)| \simeq A_x \left| \hat{S}_0 \left(\frac{\nu}{\delta_x} \right) \right| \left(\frac{\nu}{\nu_{p_0}} \right)^{\gamma_x} \tag{13}$$

is the amplitude spectrum of a Gaussian derivative wavelet defined as a derivative and dilated version of $S_0(t)$ according to

$$B_x(t) \sim \tilde{B}_x(t) \propto \frac{d^{\gamma_x}}{dt^{\gamma_x}} S_0(\delta_x t - T), \tag{14}$$

which can be used to assess the acoustic waveform in the time domain when $\nu_{p_x} \simeq \nu_{p_0}$. Note that T is introduced as a time sift related to the travel time. The fractional-derivative order, γ_x, is determined by an optimization procedure based on a simulated annealing method to optimize the normalized correlation coefficient between $B_x(t)$ and $\tilde{B}_x(t)$. The time-scale factor is then determined by $\delta_x = \sqrt{\beta_0/(\beta_0 + \gamma_x)}$ when the source signal is a Gaussian derivative wavelet or as a second free parameter in the optimization procedure.

B. Theoretical waveform approximation

The Lax's effective theory is used to model the propagation of a Gaussian derivative source wavelet. To cover different frequency ranges, three peak frequencies are considered: $\nu_{p0}/2$, ν_{p0}, and $3\nu_{p0}$ (Fig. 4), corresponding to a ratio with the bubble resonance frequency of 77.5, 155, and 465, respectively. The propagation distance is set to the maximum distance of 0.74 m, which is available in the experiments.

With $\beta_0 = 4$, the source wavelet is characterized by a symmetrical shape and five extrema. For a peak frequency of 155 kHz, the transmitted waveform determined from the analytical method is in agreement with the theoretical waveform based on the Lax's theory: the correlation coefficient is 0.992 and the additional derivative parameter $\gamma = 1.172$ is larger than one, i.e., the waveforms have theoretically seven peaks but only six dominate because the seventh peak, whose amplitude increases with γ, is too weak to be observed [Fig. 4(a)]. For $\nu_{p_0} = 310$ kHz, the analytical and theoretical waveforms are in good agreement. The correlation coefficient is close to one and $\gamma = 0.678$: for $0 < \gamma \leq 1$, the waveforms have six peaks and the sixth peak is weak when $\gamma = 0.678$ [Fig. 4(b)]. For a peak frequency of 930 kHz, the analytical and theoretical waveforms are in

https://doi.org/10.1121/10.0022256

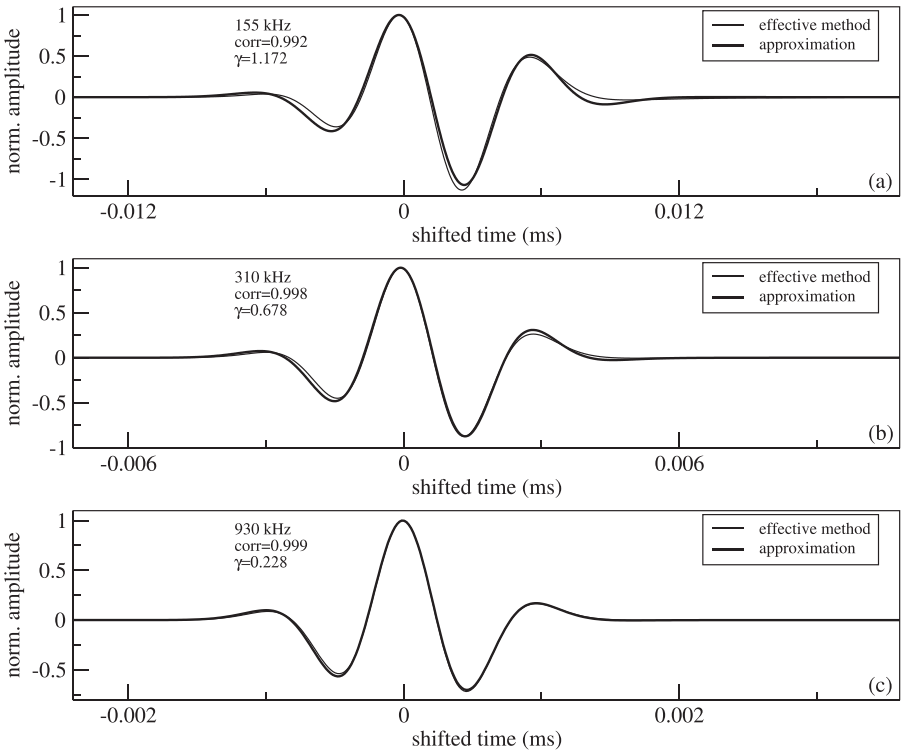

FIG. 4. (a)–(c) Theoretical waveforms based on the effective model (thin curves) and Gaussian derivative wavelet method (bold curves) for three different peak frequencies are displayed. The propagation distance is $x = 0.74$ cm.

very good agreement with a correlation coefficient about one and $\gamma = 0.228$: this derivative parameter is low, associated with a sixth peak that is too weak to be observed, and means that the waveform tends to be similar to the source wavelet, in agreement with the effective attenuation coefficient and phase velocity that become asymptotically constant at high frequencies.

As a first approach, the quality of the analytical approximation is quantified by the correlation coefficient and has been explained in a mathematical sense in Sec. III A. An acoustics interpretation may be related to the fractional order derivative because time- and space-fractional wave equations are commonly used to describe lossy media characterized by a power-law response in frequency (Zhao and McGough, 2018), i.e., by an attenuation $\alpha(\omega) = \alpha_0|\omega|^y$, where $\alpha_0 > 0$ and $0 \leq y \leq 2$ are constants (Chen and Holm, 2003). In particular, the exponent y ranges between 1 and 2 for most lossy media (Szabo, 1994), $y = 1$ for attenuation of seismic waves in rocks and sediments at frequencies larger than a cutoff frequency (Futterman, 1962), and $y = 0$ applies primarily to electromagnetic waves in the high frequency limit (Holm and Sinkus, 2010; Szabo, 1994). For the bubbly water discussed in the present paper, a weakly frequency dependent loss, i.e., $y \simeq 0$, is also observed at high frequencies and related to a fractional-derivative parameter. Fractional order derivatives are nonlocal operators in contrast to integer order derivatives in the sense that they depend on the past history of motion and have memory (Holm, 2015; Holm and Sinkus, 2010): this may explain the increase in the additional peak amplitude in the acoustic waveform when dispersion increases (Fig. 4). Multiple scattering may represent such a memory and be used to model wave propagation in random media (Garnier and Sølna, 2010; Lambert *et al.*, 2015). A simple criterion to determine whether multiple scattering occurs in the bubbly water is a propagation distance, x, larger than few scattering mean free paths, l_s (Foldy, 1945): actually, $x \leq 0.74$ m and $l_s \simeq 1$ m, i.e., memory effects may not be explained by multiple scattering in the present experiment, and other mechanisms should be considered (Caputo and Mainardi, 1971). However, these are preliminary explanations only and the waveform approximation is mainly phenomenological at this stage.

IV. APPLICABILITY OF THE METHOD

A. Experimental waveform approximation

The source signal is the experimental signal, $S_0(t)$ [Fig. 5(b1)], which is not a theoretical Gaussian derivative source wavelet. In addition, the experimental bubbly water is dynamic and may be not perfectly homogeneous, i.e., its effective properties may change temporally and spatially. The aim is quantifying the experimental waveform changes across the experimental bubbly water by the use of the additional derivative order, γ_x, determined according to the analytical approximation developed in the present paper.

The approach highlights a linear increasing trend of γ_x with x in very good agreement with the theoretical results [Fig. 5(a1)]. Actually, the agreement occurs up to the sixth bubble cloud located at $x_0 = 0.5$ m, which may be associated with a different regime of the bubble release during the

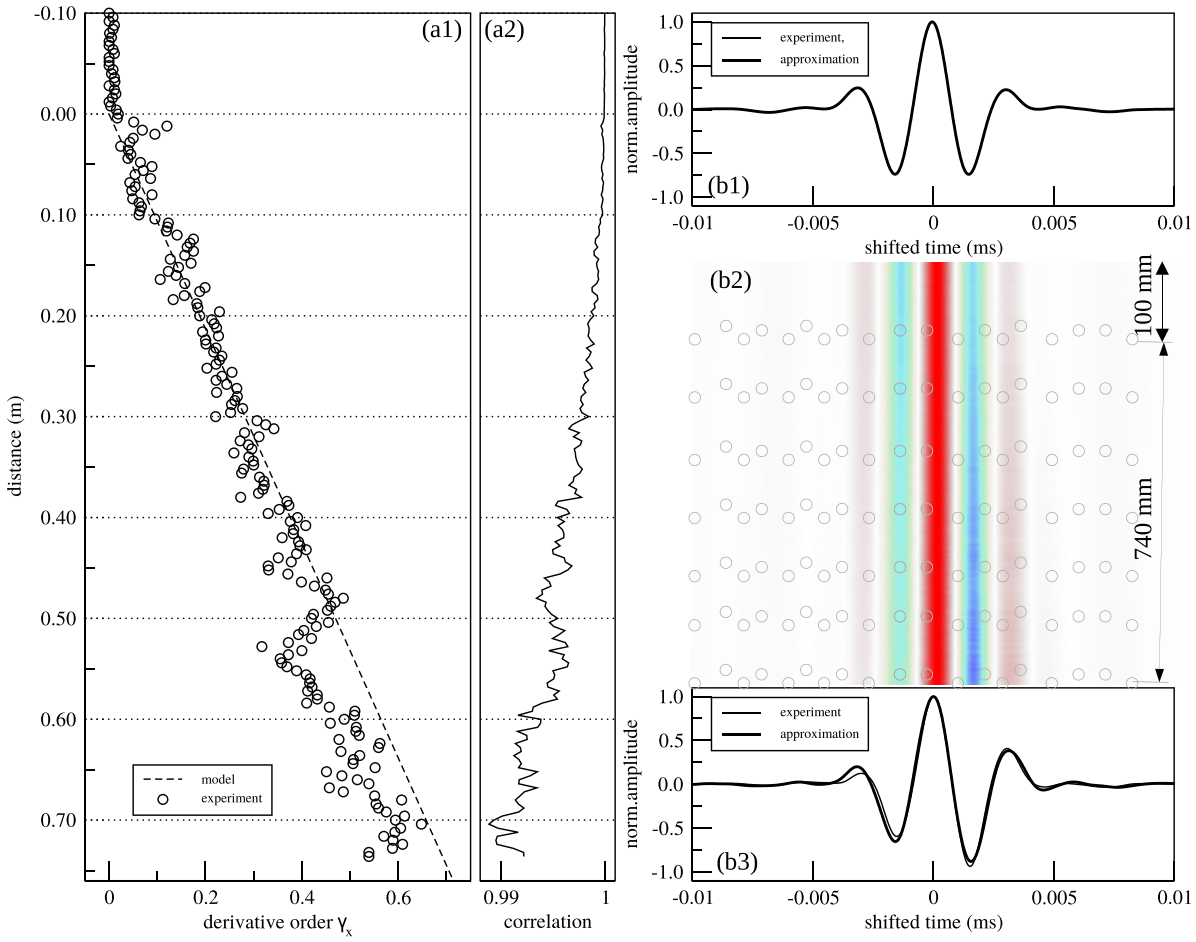

FIG. 5. (Color online) (a1) Additional derivative order, γ_x, across the experimental bubbly water (circles) and theoretical linear fit (dashed line), (a2) correlation coefficient between the experiment and approximated waveforms, (b1) experiment and approximated source signal, $S_0(t)$, (b2) approximated waveforms $(d^{\gamma_x}/dt^{\gamma_x})S_0(\delta_x t - T)$ with $\delta_x = \sqrt{\beta_0/(\beta_0+\gamma_x)}$, and (b3) last experiment and approximated waveforms (thin and bold curves, respectively) for $x = 0.74$ m are shown.

experiments. The approximated waveforms associated with γ_x highlight the progressive loss of symmetry of $S_0(t)$ when x increases [Fig. 5(b2)]. The correlation coefficient between the measured $B_x(t)$ and the approximation $\tilde{B}_x(t)$ waveforms is better than 0.99 [Fig. 5(a2)]. At the maximum distance $x = 0.74$ m, available in the measurements, the measured and approximated waveforms are in good agreement with a $S_0(t)$ shape modification quantified by $\gamma_x \simeq 0.6$ [Fig. 5(a1)]. It is expected that at larger distances, larger values of γ_x may be reached, which are associated with stronger changes of the acoustic waveforms but also a lower quality of the approximation based on $\tilde{B}_x(t)$. This point can be checked based on a modeling approach where larger distances and a wide range of different bubbly waters can be considered.

B. Extension to general bubbly waters

Previously, it has been shown numerically that the method is associated with a correlation coefficient larger than 0.99 when the source peak frequency is larger than 155 kHz for the bubbly water considered in the present study. Similar results have been highlighted experimentally with a 310 kHz source peak frequency and distances $x \leq 0.74$ m. To extend this study to different dispersive media, a numerical approach has been performed on 100 different bubbly waters with r_0 in the range 0.4–4 mm and ϕ in the range 0.05%–0.5% for $x = 1$ and 10 m, respectively. For each case, the correlation coefficient quantifies the quality of the approximation [Figs. 6(a1) and 6(b1), respectively].

An arbitrary threshold is fixed to the correlation coefficients with a minimum value of 0.97. The quality of the approximation is illustrated by the theoretical and approximated waveforms at $x = 1$ m [Fig. 6(a2), thin and bold curves, respectively] associated with $r_0 = 1.2$ mm and $\phi = 0.25\%$ [Fig. 6(a1), star]: the correlation coefficient is 0.975 for an additional derivative order, γ_x, as high as 1.957. At a larger propagation distance, the applicability of the method requires a larger bubble radius and lower density of bubbles in water, as illustrated at $x = 10$ m with $r_0 = 3.6$ mm and $\phi = 0.10\%$ [Fig. 6(b2), where the correlation coefficient is 0.995 for an additional derivative order $\gamma_x = 1.068$.

In addition, the larger the source peak frequency relative to the resonance frequency of a bubble, the larger is the coefficient correlation, which means that the applicability range of the method can be extended by increasing the source frequency.

https://doi.org/10.1121/10.0022256

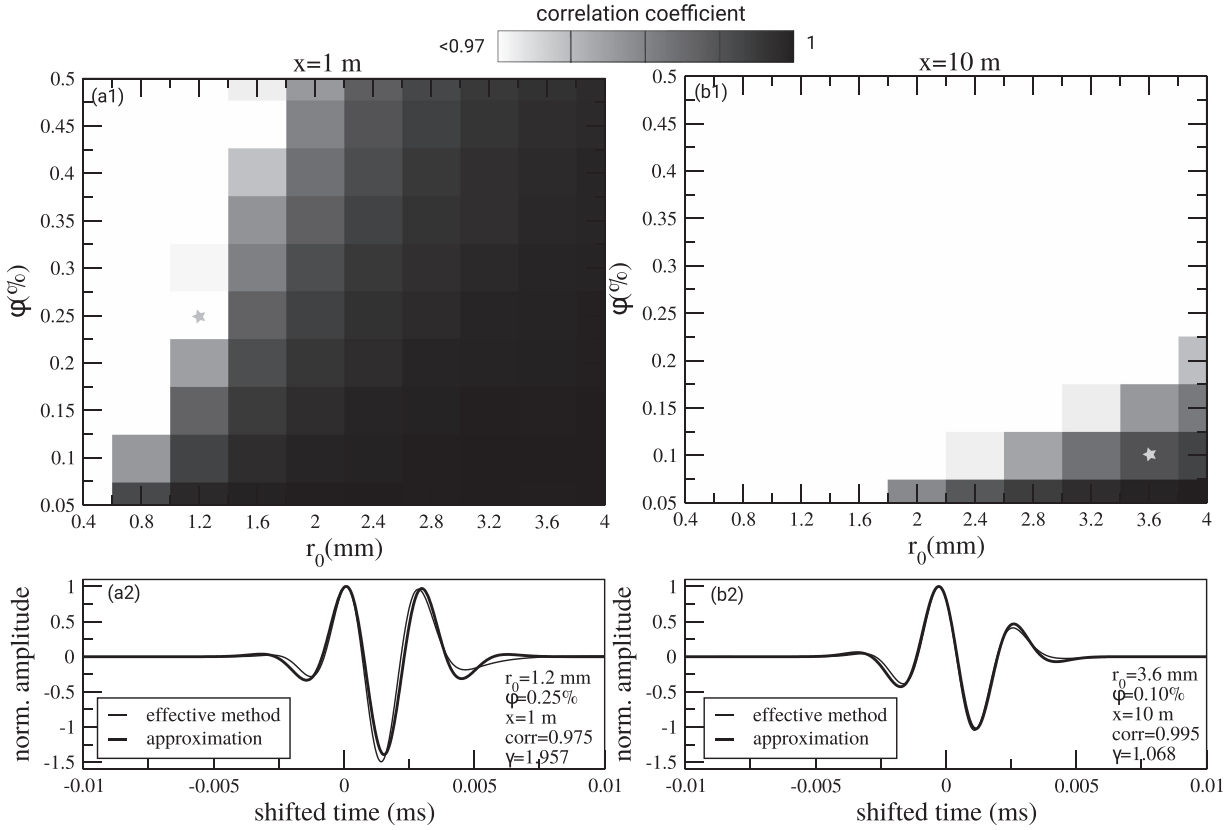

FIG. 6. (a1), (b1) Maps of normalized correlation coefficients for $x = 1$ and 10 m, respectively (best correlation in black), (a2), (b2) waveforms of the acoustic signals modeled with the Lax's model (thin curves) for a volume fraction ϕ of r_0 radius bubbles, identified on the maps by the stars, and approximations (bold curves) are displayed.

V. CONCLUSION

The present work describes acoustic experiments and analytical developments to quantify waveform changes of a Gaussian derivative source wavelet, $S_0(t)$, characterized by a peak frequency, ν_{p_0}, and derivative order, β_0, inside a dispersive medium. The main assumption of the approach deals with the peak frequency, ν_{p_x}, of the waveform, $B_x(t)$, measured at the distance x, which is $\nu_{p_x} \simeq \nu_{p_0}$. It is shown that this condition is satisfied for acoustic experiments performed with 1.6 mm radius bubbles composing a bubbly water with a gas volume fraction 20%, and for $\nu_{p_0} = 310$ kHz and $x \leq 0.74$ m. Analytical developments show that if $\nu_{p_x} \simeq \nu_{p_0}$, the acoustic waveform can be approximated by $\tilde{B}_x(t) \propto (d^{\gamma_x}/dt^{\gamma_x}) S_0(\delta_x t - T)$, where γ_x is an additional fractional-derivative order determined by the use of an optimization procedure. The time-scale factor is $\delta_x = \sqrt{\beta_0/(\beta_0 + \gamma_x)}$ for a Gaussian derivative source wavelet; otherwise, it is a second free parameter for the optimization method. The approach applied to the experiments highlights a linear increase of γ_x with x from 0 to 0.6 with a very good agreement between numerical and experimental waveforms. A preliminary acoustics interpretation is discussed in the framework of fractional order derivatives, based on a power-law response in frequency and a time-domain memory.

To check the applicability of the method to more general conditions, the approach has been extended numerically to different source peak frequencies, different distances of propagation, and different bubbly waters characterized by the Lax's effective medium theory. The aim was using the theoretical attenuation coefficient, $\alpha(\nu)$, and phase velocity, $\alpha(\nu)$, of the dispersive medium to model the acoustic waveform propagation and quantify the application of the approximation, $B_x(t) \simeq \tilde{B}_x(t)$, by a normalized correlation coefficient. Two hundred different configurations of bubbly waters in large ranges of bubble radius in 0.4–4 mm and volume fraction in 0.05%–0.5% have been considered for $x = 1$ and 10 m: the maps of correlation coefficients highlight that the domain of applicability of the method is very large at short distances and focuses at large distances to low concentrations of large bubbles. A threshold of 0.97 on the correlation coefficient corresponds to maximum derivative orders about two, related to significant shape changes. The applicability of the method, focused in the present work on air bubbles in water, may be extended to other dispersive media, assuming that the peak frequency of the dispersed acoustic waveform remains constant to the peak frequency of the source signal.

Similar circumstances of bubbly waters may exist in the close vicinity of active gas seeps, for instance, where bubbles can occur at volumetric void fractions as low as 0.01% with diameters up to 4 mm and sounded by the use of a very high frequency echosounder (Wang *et al.*, 2016). In such natural environments, the present work may motivate future

works on underwater communication by contributing to acoustic quantification of gas bubbles in the ocean water column. More generally, it introduces a fractional-derivative order in the time domain of potential interest when modeling acoustic wave propagation in dispersive media.

ACKNOWLEDGMENTS

The author would like to thank Dr. Stéphan Ker for discussions on anelastic media in marine geophysics and Bruno Kergosien for his contribution in the design of the experimental setup.

AUTHOR DECLARATIONS

Conflict of Interest

The author has no conflicts of interest to disclose.

DATA AVAILABILITY

The data that support the findings of this study are available from the author upon reasonable request.

Ainslie, M. A., and Leighton, T. G. (**2011**). "Review of scattering and extinction cross-sections, damping factors, and resonance frequencies of a spherical gas bubble," J. Acoust. Soc. Am. **130**(5), 3184–3208.

Ammari, H., Fitzpatrick, B., Gontier, D., Lee, H., and Zhang, H. (**2018**). "Minnaert resonances for acoustic waves in bubbly media," Ann. Inst. H. Poincaré C, Anal. Non Linéaire **35**, 1975–1998.

Anderson, V. C. (**1950**). "Sound scattering from a fluid sphere," J. Acoust. Soc. Am. **22**(4), 426–431.

Ando, K., Colonius, T., and Brennen, C. E. (**2009**). "Improvement of acoustic theory of ultrasonic waves in dilute bubbly liquids," J. Acoust. Soc. Am. **126**(3), EL69–EL74.

Caputo, M., and Mainardi, F. (**1971**). "A new dissipation model based on memory mechanism," Pure Appl. Geophys. **91**, 134–147.

Chen, W., and Holm, S. (**2003**). "Modified Szabo's wave equation models for lossy media obeying frequency power law," J. Acoust. Soc. Am. **114**(5), 2570–2574.

Commander, K. W., and Prosperetti, A. (**1989**). "Linear pressure waves in bubbly liquids: Comparison between theory and experiments," J. Acoust. Soc. Am. **85**(2), 732–746.

Devaud, M., Hocquet, T., Bacri, J.-C., and Leroy, V. (**2008**). "The Minnaert bubble: An acoustic approach," Eur. J. Phys. **29**(6), 1263–1285.

Doc, J.-B., Conoir, J.-M., Marchiano, R., and Fuster, D. (**2016**). "Nonlinear acoustic propagation in bubbly liquids: Multiple scattering, softening and hardening phenomena," J. Acoust. Soc. Am. **139**(4), 1703–1712.

Duraiswami, R., Prabhukumar, S., and Chahine, G. L. (**1998**). "Bubble counting using an inverse acoustic scattering method," J. Acoust. Soc. Am. **104**(5), 2699–2717.

Duro, V., Rajaona, D. R., Décultot, D., and Maze, G. (**2011**). "Experimental study of sound propagation through bubbly water: Comparison with optical measurements," IEEE J. Ocean. Eng. **36**(1), 114–125.

Fan, Y., Li, H., Xu, C., and Zhou, T. (**2019**). "Influence of bubble distributions on the propagation of linear waves in polydisperse bubbly liquids," J. Acoust. Soc. Am. **145**(1), 16–25.

Foldy, L. (**1945**). "The multiple scattering of waves," Phys. Rev. **67**, 107–119.

Fox, F. E., Curley, S. R., and Larson, G. S. (**1955**). "Phase velocity and absorption measurements in water containing air bubbles," J. Acoust. Soc. Am. **27**(3), 534–539.

Frinking, P. J., de Jong, N., and Cespedes, E. I. (**1999**). "Scattering properties of encapsulated gas bubbles at high ultrasound pressures," J. Acoust. Soc. Am. **105**(3), 1989–1996.

Fuster, D., Conoir, J.-M., and Colonius, T. (**2014**). "Effect of direct bubble-bubble interactions on linear-wave propagation in bubbly liquids," Phys. Rev. E **90**(6), 063010.

Futterman, W. I. (**1962**). "Dispersive body waves," J. Geophys. Res. **67**(13), 5279–5291, https://doi.org/10.1029/JZ067i013p05279.

Garnier, J., and Sølna, K. (**2010**). "Effective fractional acoustic wave equations in one-dimensional random multiscale media," J. Acoust. Soc. Am. **127**(1), 62–72.

Goertz, D., Frijlink, M., Voormolen, M., de Jong, N., and van der Steen, A. (**2006**). "High frequency attenuation measurements of lipid encapsulated contrast agents," Ultrasonics **44**, e131–e134.

Hoff, L., Sontum, P. C., and Hovem, J. M. (**2000**). "Oscillations of polymeric microbubbles: Effect of the encapsulating shell," J. Acoust. Soc. Am. **107**(4), 2272–2280.

Holm, S. (**2015**). "Four ways to justify temporal memory operators in the lossy wave equation," in *2015 IEEE International Ultrasonics Symposium (IUS)*, Taipei, Taiwan (IEEE, New York), pp. 1–4.

Holm, S., and Sinkus, R. (**2010**). "A unifying fractional wave equation for compressional and shear waves," J. Acoust. Soc. Am. **127**(1), 542–548.

Ker, S., and Le Gonidec, Y. (**2018**). "Fractional integration of seismic wavelets in anelastic media to recover multiscale properties of impedance discontinuities," Geophysics **83**, 61–71.

Lambert, S. A., Näsholm, S. P., Nordsletten, D., Michler, C., Juge, L., Serfaty, J.-M., Bilston, L., Guzina, B., Holm, S., and Sinkus, R. (**2015**). "Bridging three orders of magnitude: Multiple scattered waves sense fractal microscopic structures via dispersion," Phys. Rev. Lett. **115**(9), 094301.

Lax, M. (**1951**). "Multiple scattering of waves," Rev. Mod. Phys. **23**, 287–310.

Le Gonidec, Y., Gibert, D., and Proust, J.-N. (**2002**). "Multiscale analysis of waves reflected by complex interfaces: Basic principles and experiments," J. Geophys. Res. **107**(B9), 2184, https://doi.org/10.1029/2001JB000558

Leroy, V., Strybulevych, A., and Page, J. (**2008**). "Sound velocity and attenuation in bubbly gels measured by transmission experiments," J. Acoust. Soc. Am. **123**, 1931–1940.

Liang, B., Zou, X., and Cheng, J. (**2008**). "Effective medium method for sound propagation in a soft medium containing air bubbles," J. Acoust. Soc. Am. **124**(3), 1419–1429.

Padilla, A. M., and Weber, T. C. (**2021**). "Acoustic backscattering observations from non-spherical gas bubbles with *ka* between 0.03 and 4.4," J. Acoust. Soc. Am. **149**(4), 2504–2519.

Rubinstein, J. (**1985**). "Bubble interaction effects on waves in bubbly liquids," J. Acoust. Soc. Am. **77**(6), 2061–2066.

Silberman, E. (**1957**). "Sound velocity and attenuation in bubbly mixtures measured in standing wave tubes," J. Acoust. Soc. Am. **29**(8), 925–933.

Suiter, H. (**1992**). "Pulse length effects on the transmissivity of bubbly water," J. Acoust. Soc. Am. **91**(3), 1383–1387.

Szabo, T. L. (**1994**). "Time domain wave equations for lossy media obeying a frequency power law," J. Acoust. Soc. Am. **96**(1), 491–500.

Valier-Brasier, T., Conoir, J.-M., Coulouvrat, F., and Thomas, J.-L. (**2015**). "Sound propagation in dilute suspensions of spheres: Analytical comparison between coupled phase model and multiple scattering theory," J. Acoust. Soc. Am. **138**(4), 2598–2612.

Wang, B., Socolofsky, S. A., Breier, J. A., and Seewald, J. S. (**2016**). "Observations of bubbles in natural seep flares at MC 118 and GC 600 using *in situ* quantitative imaging," J. Geophys. Res.: Oceans **121**(4), 2203–2230, https://doi.org/10.1002/2015JC011452.

Wang, Y. (**2015**). "Generalized seismic wavelets," Geophys. J. Int. **203**, 1172–1178.

Wilson, P. S., Roy, R. A., and Carey, W. M. (**2005**). "Phase speed and attenuation in bubbly liquids inferred from impedance measurements near the individual bubble resonance frequency," J. Acoust. Soc. Am. **117**(4), 1895–1910.

Ye, Z. (**1997**). "Acoustic dispersion and attenuation in many spherical scatterer systems and the Kramers-Kronig relations," J. Acoust. Soc. Am. **101**, 3299–3305.

Zhao, X., and McGough, R. J. (**2018**). "Time-domain analysis of power law attenuation in space-fractional wave equations," J. Acoust. Soc. Am. **144**(1), 467–477.